RSC Advances

PAPER

View Article Online
View Journal | View Issue

Cite this: *RSC Adv.*, 2016, **6**, 90674

Strongly anisotropic thermal and electrical conductivities of a self-assembled silver nanowire network

Zhe Cheng,*[ab] Meng Han,[a] Pengyu Yuan,[a] Shen Xu,[a] Baratunde A. Cola[b] and Xinwei Wang[a]

Heat dissipation issues are emerging challenges in the field of flexible electronics. Thermal management of flexible electronics creates a demand for flexible materials with highly anisotropic thermal conductivity, which work as heat spreaders to remove excess heat in the in-plane direction and as heat shields to protect human skin or device components under them from heating. To solve these challenges, this study proposes a self-assembled silver nanowire network with high thermal and electrical anisotropy. We measured the in-plane thermal conductivity of the network along the axial direction of silver nanowires as 37 W m^{-1} K^{-1} and the cross-plane thermal conductivity as only 0.36 W m^{-1} K^{-1}. The results of measurements of electrical and thermal conductivities suggest that abundant wire–wire contacts strongly impede thermal transport. The excellent alignment of nanowires results in the same anisotropy ratio of three for both thermal and electrical conduction in the two in-plane directions. The ratio remains unchanged as the temperature decreases to 50 K, indicating that wire–wire contacts lower the thermal and electrical conduction in the two directions to the same extent, and their effect is independent of temperature. In addition, phonon softening markedly reduces the Debye temperatures of the network, which are fitted from electrical resistivity data. As a result of phonon thermal conduction and localized phonon assisted energy transfer near boundaries, the Lorenz numbers of the film in the two directions, which are approximately the same, are larger than the Sommerfeld value at room temperature and decrease as the temperature decreases because of small angle scattering and the reduced number of phonons. This nanowire network provides a candidate solution to the emerging challenges of the thermal management of flexible electronics.

Received 11th August 2016
Accepted 16th September 2016

DOI: 10.1039/c6ra20331k

www.rsc.org/advances

1. Introduction

The rapid development of flexible electronics motivates the research of thermal management in these electronics.[1–3] Unlike traditional electronics built on high thermal conductivity substrates such as crystalline silicon, the electrical elements of flexible electronics are built on flexible polymer substrates with thermal conductivity two to three orders of magnitude lower. Even though the power levels of these electrical elements are much lower than those of large-scale integrated circuits, heat dissipation issues in flexible electronics, which lower the stability and shorten the life of these electronics, are some of the emerging challenges in the thermal management of electronics.[1,3] Moreover, flexible electronics frequently interacts with human skin, which needs to be protected from hot-spots generated by electrical elements.[4–6] These two factors create a demand for new flexible materials with highly anisotropic thermal conductivity for thermal management, in which the in-plane thermal conductivity is significantly larger than the cross-plane thermal conductivity. With these properties, the materials work as heat spreaders to remove excess heat in the in-plane direction and as heat shields to protect human skin or device components under them from heating. With the increasing requirements of customer experience in the design of flexible, wearable and portable electronics, the anisotropic materials provide a solution to prevent human skin from feeling any temperature variation in these electronics.

A candidate of these highly anisotropic flexible materials is silver nanowire, which is flexible and non-toxic with high thermal and electrical conductivity along the axial direction.[7–11] Individual nanowires, however, need to be scaled up as functional materials. Methods usually used to scale up silver nanowires are dip-coating, spinning, or spraying coating.[10–12] Nanowire networks fabricated by these methods are randomly oriented. Recently the large-scale self-assembly of nanowires provides a solution to fabricating highly aligned nanowire

[a]*Department of Mechanical Engineering, 2010 Black Engineering Building, Iowa State University, Ames, Iowa, 50011, USA. E-mail: zcheng@gatech.edu; Tel: +1-515-520-4484*

[b]*George W. Woodruff School of Mechanical Engineering, Georgia Institute of Technology, Atlanta, Georgia 30332, USA*

networks.[13] The thermal and electrical properties of this self-assembled network are determined by not only the size effect of typical nanostructures but also the alignment of nanowires and contacts among a large number of wires, the latter two of which are the special features of this network. Additionally, in the in-plane directions, the aligned nanowire network facilitates directional control of thermal energy transport.

In this work, we report a self-assembled silver-nanowire network for thermal management applications. To understand the physics of electrical and thermal transport in this special structure, we applied the transient electro-thermal (TET) technique to measure thermal and electrical conductivities in two in-plane directions from room temperature down to 50 K. We also used the photothermal-radiation (PTR) technique and the photoacoustic (PA) technique to determine the cross-plane thermal conductivity at room temperature. It should be pointed out that our work presents a pioneering effort to study this aligned structure of the metallic nanowire network and the effect of abundant wire–wire contacts on thermal and electrical conduction, and this nanowire network provides a candidate solution for the thermal management of flexible electronics.

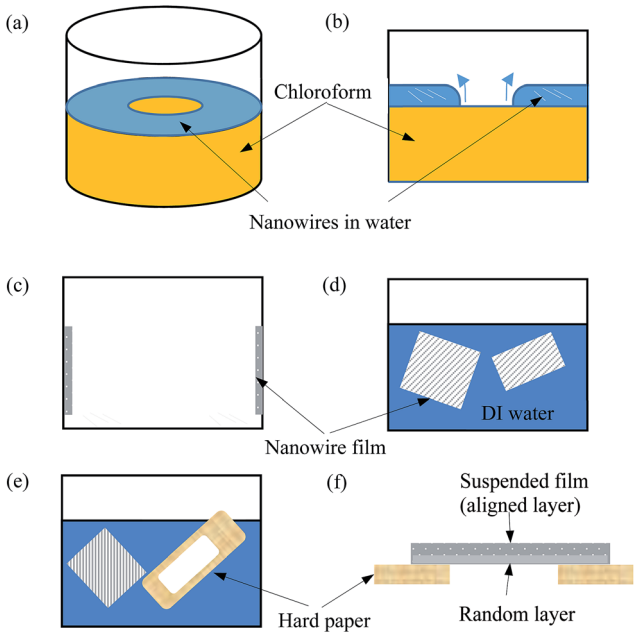

Fig. 1 The schematic diagram of the self-assembly process. (a and b) The self-assembly method and principle. (c) The film is coated on the wall of the glass beaker. (d) The film is suspended in DI water. (e) Hard paper is used to draw up the nanowire film. (f) The film is dried in air.

2. Sample preparation and characterization

2.1 Sample preparation

For the preparation of the silver nanowire network, silver nanowires are self-assembled by a three-phase method (oil–water–air).[13] Purchased from ACS Material, LLC, the silver nanowires, with an average diameter of 50 nm and an average length of 200 μm, are dispersed in deionized (DI) water and used as received. A schematic diagram of the self-assembly process is depicted in Fig. 1. First, a clean beaker is half-filled with chloroform. Then, silver nanowire solution is dropped on the chloroform surface. The amount of dropped solution is controlled so that the water phase and the air phase cover approximately 80% and 20% of the chloroform surface. As shown in Fig. 1(a) and (b), evaporation of the chloroform drives the water layer to move, which results in the self-assembly of silver nanowires at the surface of the water layer. The evaporation of chloroform at the chloroform–air surface drives the moving of chloroform–water surface which consists of chloroform and silver nanowires. During this process, the silver nanowires are transferred from the water–chloroform interface to the water–air interface through the water–air–chloroform interface. The aligned film first forms at the water–air–beaker wall because of capillary force and the nanowires are aligned parallel to the beaker wall at the water–air surface. When the nanowires are well aligned in the water–air interface, visible light cannot "see" the surface roughness because the wavelength of visible light is 400–700 nm which is much larger than the nanowire diameter (50 nm). As a result, the self-assembled nanowire network is a mirror-like film at the top of the water phase that can be coated on glass slides, silicon wafers, or textiles.

After the film is assembled, chloroform is replaced by water in the fabrication of dry samples for the TET measurements. Fig. 1(c) and (d) show that the film is coated on the beaker wall after chloroform is removed, and the film is suspended again after DI water is added. Fig. 1(e) shows that the film is attached to hard paper whose central part is cut off. After being drawn up from water, the film is dried in air for several hours. The film covering the central "window" of the paper is suspended in air, as shown in Fig. 1(f). Finally, the dry and suspended film is cut into strips for the TET measurements. One needs to be mentioned is that during the self-assembly process, some nanowires dispersed in the water phase accumulatively attach to the bottom of the assembled film due to capillary force and van der Waals force, which forms a randomly oriented layer on the bottom of the network as shown in Fig. 1(f).

2.2 Structure characterization

The structure of the self-assembled silver nanowire film is characterized by scanning electron microscopy (SEM) and X-ray diffraction (XRD). As illustrated in Fig. 2(a) and (b), the film is composed of two layers: one aligned layer and one randomly oriented layer. Fig. 2(b) defines directions that will be used later. The cross-plane direction is the direction through the film. Parallel and perpendicular directions are parallel and perpendicular to the axial direction of the aligned silver nanowires. Fig. 2(c) and (d) show the SEM graphs of the aligned and randomly oriented layers, respectively. This aligned structure results in the anisotropic properties of the film. The existence of the randomly oriented layer and the layered structure lead to large difference in the properties in the cross-plane and

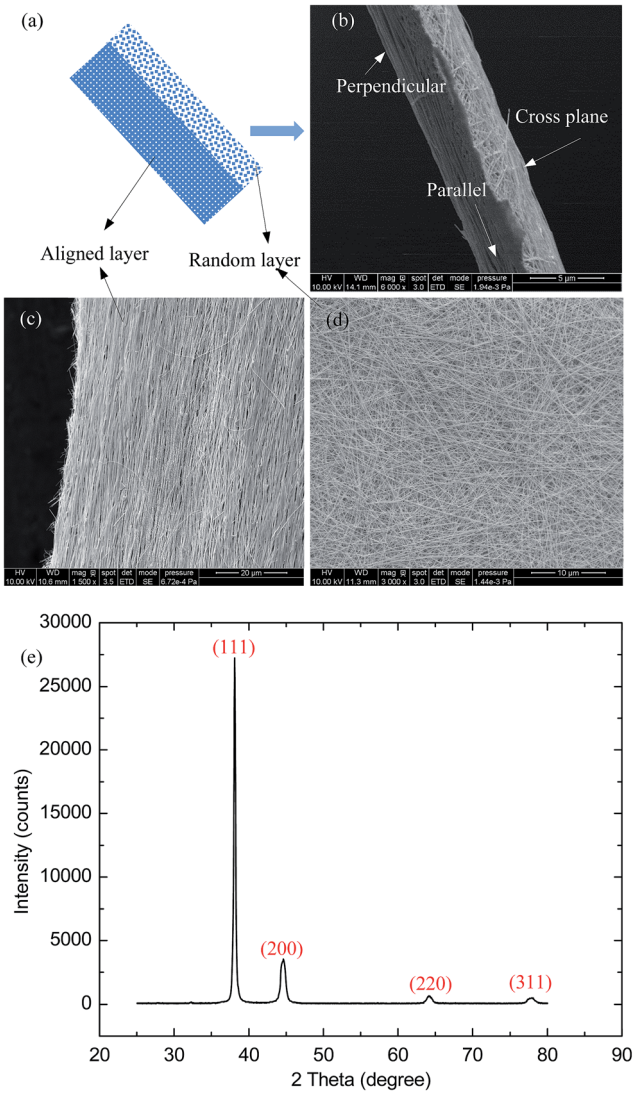

Fig. 2 (a) The bilayer structure of the nanowire film. (b) The SEM graph of the film cross section and the definition of the three directions. (c and d) The SEM graphs of the aligned and random layers. (e) The XRD pattern of the film.

perpendicular directions of the network. The nanowires were also studied by XRD, whose pattern is shown in Fig. 2(e). The crystal sizes calculated from the peaks in the pattern are 46 nm in the (111) direction, 14 nm in the (200) direction, 14 nm in the (220) direction, and 11 nm in the (311) direction. All of these sizes are smaller than the average diameter of the nanowires, which indicates that the silver nanowires are polycrystalline. The lattice plane spacing for peaks (111), (200), (220), and (311) are 2.3618 Å, 2.0314 Å, 1.4519 Å, and 1.2277 Å, respectively; and the corresponding lattice constants are 4.09 Å, 4.06 Å, 4.11 Å, and 4.07 Å, respectively.

2.3 Thermal and electrical characterization

For thermal and electrical measurement, the to-be-measured sample is suspended between two Al electrodes (heat sinks) after being cut into strips. The TET technique[14–18] is used to measure the thermal and electrical properties of the film strip. In the measurement, a constant electrical current is applied to the sample. The joule heat generated by the current induces a temperature increase in the sample. Electrical resistivity is proportional to temperature, so the increase in the temperature is proportional to increase in the electrical resistance of the sample and then the voltage. By measuring the voltage change, we obtain the data of temperature variation. The thermal properties of the sample are extracted by fitting the data to a theoretical thermal model. The fitted thermal conductivity is the in-plane thermal conductivity along the direction of the electrical current. To measure the thermal conductivity in the two directions, we prepare two strip-shaped samples. Specifically, the size of the sample, fabricated to measure the parallel thermal and electrical conductivity, is 1751 μm long, 38 μm wide, and 4.1 μm thick while the size of the perpendicular counterpart is 1456 μm long, 64 μm wide, and 4.5 μm thick. Additionally, the electrical currents applied to these samples are small (several mA), so all of the temperatures rises in the samples by less than 7 K. These small increases in temperature guarantee that at the wire–wire contacts, nanowires are not soldered during the measurements, which is also confirmed by the same electrical resistance before and after each measurement.

During the measurement process, convection and radiation also play important roles. To suppress the effect of air convection, the sample is placed in a vacuum chamber with its pressure below 0.5 mTorr. The effect of radiation is estimated by $(8\varepsilon_r\sigma T_0^3 L^2)/(D\pi^2)$, where ε_r is the emissivity, σ is the Stefan–Boltzmann constant, T_0 is the temperature, L is the length, and D is the thickness of the sample. If emissivity takes the value of 0.3, the maximum effects of radiation for the two measured samples are approximately 1% of those of thermal conduction, which are negligible in the measurement. From the thermal characterization data, we also obtain electrical resistance. To eliminate the effect of contact resistance, a four-point method, a schematic diagram of which is illustrated in the top inset of Fig. 3, is used to measure the electrical resistance.

In-plane thermal conductivity is characterized by the TET technique while cross-plane thermal conductivity of the film is measured by the PTR technique.[19–21] For PTR measurement, a modulated laser is used to heat the silver nanowire film coated on a glass slide. The absorbed laser energy penetrates the sample through cross-plane heat conduction and emits radiation into the environment. The amplitude and phase changes in the radiation signal, which monitor the temperature change of the sample surface, are detected. The thermal conductivity of the sample is extracted by fitting these data to a theoretical thermal model. In this work, the modulated laser beam frequencies range from 17 Hz to 20 kHz.

Cross-plane thermal conductivity is also confirmed by the PA technique.[22,23] This technique uses a periodically modulated laser that heats the sample surface, generating an acoustic wave in the gas adjacent to the sample surface because of the pressure and temperature variation of the gas. A microphone detects the amplitude and phase shift of the acoustic signal. Cross-plane thermal conductivity is extracted by fitting the phase shift at a range of frequencies to a theoretical thermal model. In

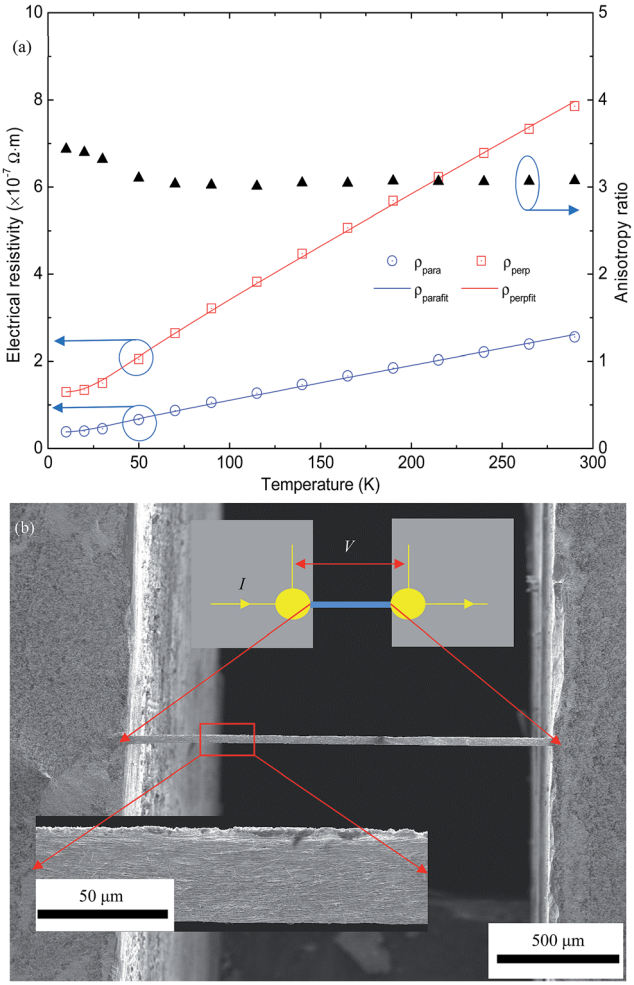

Fig. 3 (a) The temperature-dependent electrical resistivity in the parallel and perpendicular directions. The right coordinate axis is the anisotropy ratio of electrical conductivity. (b) The SEM graph of a sample suspended between two electrodes. The top inset shows the four-point method for electrical characterization. The bottom inset shows the magnified SEM graph of the sample surface.

this work, the silver nanowire film is coated on a glass slide, and 150 nm Ti is coated on the film as a transducer. Measurement frequencies range from 100 Hz to 4000 Hz. In this frequency range, the maximum penetration depths in the cross- and in-plane directions are 0.053 and 0.47 mm, respectively, which are smaller than the laser beam size (1 mm). Therefore, we assume the cross-plane heat conduction is one-dimensional.

3. Results and discussion

3.1 Anisotropic electrical resistivity

The electrical resistivity of the film in the parallel and perpendicular directions is measured by the four-point method, and the results are shown in Fig. 3. Here, we define the anisotropy ratio of electrical conductivity as $\eta_e = \sigma_{para}/\sigma_{perp} = \rho_{perp}/\rho_{para}$, where σ_{para} and σ_{perp} represent electrical conductivity in the parallel and perpendicular directions, respectively. According to Matthiessen's rule and the Bloch–Grüneisen formula,[24] the electrical resistivity of the film is $\rho = \rho_0 + \rho_{el-ph}$. Here, ρ_0 is the residual electrical resistivity, which is temperature independent. Its value is the resistivity value when the temperature approaches zero. ρ_{el-ph} can be expressed as

$$\rho_{el-ph} = \alpha_{el-ph}\left(\frac{T}{\theta}\right)^n \int_0^{\theta/T} \frac{x^n}{(e^x - 1)(1 - e^{-x})}\,dx, \quad (1)$$

where α_{el-ph} is the electron–phonon coupling parameter, θ is the Debye temperature, and n generally takes the value of 5 for nonmagnetic metals.[25] By fitting experimental data to the Bloch–Grüneisen formula, the Debye temperatures of the film in the parallel and perpendicular directions are 107 K and 132 K, respectively. Both are smaller than the Debye temperatures of bulk silver and single silver nanowires (235 K and 151 K).[7] The low Debye temperature is due to three factors: surface phonon softening in the silver nanowires, which has also been observed in other nanostructures,[7,26–30] quasi-ballistic electron transport and the abundant wire–wire contacts. The missing bonds of atoms at defects, grain boundaries, and surfaces, lead to changes in phonon modes and reductions in the vibration frequency, which results in a reduced Debye temperature. Moreover, electron mean free path in bulk silver is comparable or larger than the grain size in silver nanowires in this work. The mechanism of quasi-ballistic electron transport will be discussed in detail later. Additionally, some wire–wire contacts have a thin layer of organic molecules that stabilize the suspension of silver nanowires. Electrons need to pass through this layer and scatter with locons or diffusions in this layer, which contributes to changing Debye temperature. Fig. 3 shows that the anisotropy ratio of electrical conductivity is constant when the temperature is higher than 50 K, indicating that temperature has the same effect on electron transport in both directions. As the temperature decreases below 50 K, the anisotropy ratio increases slightly. In this temperature range, electrical resistivity is no longer linear with temperature. The effect of electron–phonon scattering diminishes while that of electron-structural imperfection scattering becomes increasingly important as temperature decreases.

3.2 Anisotropic thermal conductivity

The TET technique is used to measure the thermal conductivity of the film in the two in-plane directions from room temperature to 50 K, and the results of measurements are shown in Fig. 4(a). Compared with the thermal conductivity of bulk silver, that of the self-assembled nanowire film in the "parallel" and "perpendicular" directions decreases by 91% and 97%, respectively. Compared with the thermal conductivity of the single silver nanowire, that in the two directions drop by 80% and 93%, respectively,[7] indicating that size effect and wire–wire contacts dominantly impede the thermal transport. The in-plane thermal conductivity, approximately two orders of magnitude larger than that of the flexible substrate usually used in flexible electronics, can still be enlarged significantly by reducing wire–wire contact resistance. Several possible methods include thermal annealing,[31] mechanical press,[32] metal coating,[10] and self-limited plasmonic welding.[33]

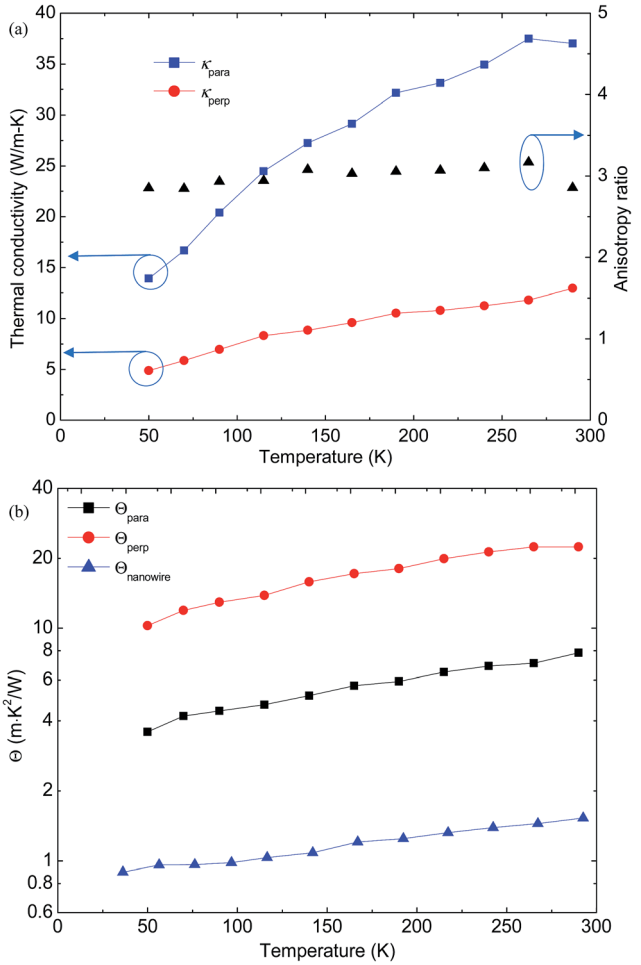

Fig. 4 (a) The thermal conductivity of the self-assembled nanowire film in two directions (parallel and perpendicular to the axial direction of the aligned silver nanowire). The right coordinate axis shows the anisotropy ratio of the thermal conductivity in these two directions. (b) The unified thermal resistivity of the film in the "parallel" and "perpendicular" directions compared to that of a single silver nanowire.[7]

The great reduction in thermal conduction is due to the abundant wire–wire contacts and porous structure. Similarly, the high anisotropy in thermal conduction is due to the special aligned structure. In the direction parallel to the axial direction of the aligned silver nanowires, electrons transfer along the nanowires in the aligned layer while in the other direction, electrons transfer through more wire–wire contacts. Electrons transfer along the silver nanowires with smaller resistance than they do through the contacts. Thus, the thermal conductivity of the film shows high thermal anisotropy. Fig. 4(a) shows that the thermal anisotropy ratio remains relatively constant as temperature decreases. The thermal conductivity in the "parallel" direction is about three times as high as that in the "perpendicular" direction. This ratio is close to the electrical anisotropy ratio, indicating that wire–wire contacts dominantly impede thermal and electrical transport and lower thermal and electrical conductivity to the same extent.

As temperature decreases, the specific heat of electrons decreases, and the electron mean free path increases. Because of the large number of structural imperfections such as wire–wire contacts, the acceleration of the mean free path is not as fast as the deceleration of specific heat. As a result, the thermal conductivity of the film in the two directions decreases as temperature decreases. Specifically, the thermal conductivity of metals can be written as $\kappa = C_v v_F^2 \tau/3$, where C_v is the volumetric heat capacity of electrons, v_F the Fermi velocity, and τ the relaxation time. At low temperatures, the volumetric heat capacity of electrons changes linearly with temperature ($C_v = \gamma T$), and γ is a constant (0.646 mJ mol^{-1} K^{-2} for silver). For silver, the Fermi velocity is 1.39 $\times$ 10^6 m s^{-1} and the electron density 5.85 $\times$ 10^{28} m^{-3}.[34] In metallic structures, both charge and energy carriers are electrons. Compared with charge transport, energy transport involves the specific heat of electrons, which is temperature dependent. Therefore, to eliminate the effect of temperature on thermal resistivity resulting from the electron heat capacity, we define unified thermal resistivity as $\Theta = T/\kappa$, which shows the effect of scattering sources on thermal resistivity, similar to electrical resistivity.[7,15] According to Matthiessen's rule, the unified thermal resistivity can be separated into two parts based on the following scattering mechanisms: the phonon scattering part and the structural scattering part ($\Theta = (3/\gamma v_F^2)(\tau_0^{-1} + \tau_{ph}^{-1}) = \Theta_0 + \Theta_{ph}$). As temperature approaches zero Kelvin, the effect of phonon–electron scattering diminishes ($\Theta_{ph} = 0$). The residual unified thermal resistivity (Θ_0) reflects the structural information of the sample. As shown in Fig. 4(b), the unified thermal resistivities of the film and a single silver nanowire decrease as temperature decreases. The residual unified thermal resistivities of the film in the "perpendicular" and "parallel" directions and the single silver nanowire are around 10.2, 3.6, and 0.9 mK^2 W^{-1}, respectively, which confirms our expectation: structural disorder results in a large residual unified thermal resistivity. For a perfect bulk crystal, the residual unified thermal resistivity should be zero.

In terms of the measurement of cross-plane thermal conductivity, Fig. 5(a) depicts the data fitting of the PTR measurement. To obtain the cross-plane thermal conductivity, we fit both the phase shift and the amplitude, which produce excellent fitting. The corresponding cross-plane thermal conductivity extracted from the phase shift and the amplitude are 0.35 W m^{-1} K^{-1} and 0.37 W m^{-1} K^{-1}, respectively. We take the average of these two values (0.36 W m^{-1} K^{-1}) as the cross-plane thermal conductivity of the film. These values are confirmed by the PA measurement. As shown in Fig. 5(b), the fit between the experimental data and the theoretical model values is excellent. The thickness we used to fit the data takes the value of the average thickness of the two TET samples (4.3 μm). The fitted cross-plane thermal conductivity is 0.40 W m^{-1} K^{-1}, which is 10% larger than that measured by PTR because the PA sample is coated with 150 nm Ti, which may enhance cross-plane thermal transport. The experimental errors of PTR and PA are 10%.

The cross-plane thermal conductivity and the thermal conductivities in the two in-plane directions at room temperature are plotted in Fig. 6 for comparison. Specifically, the cross-plane thermal conductivity is about two orders of magnitude lower

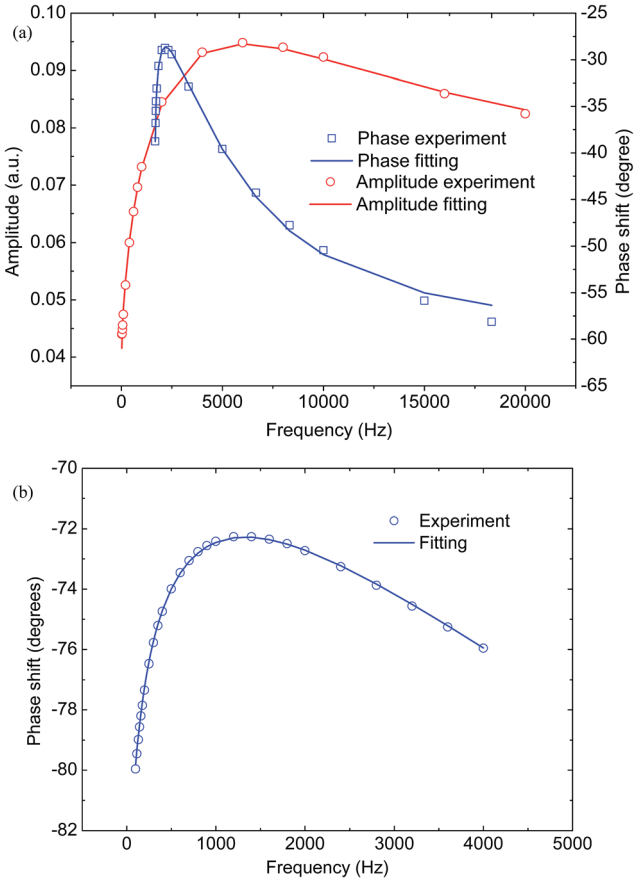

Fig. 5 (a) The experimental data and fittings of the PTR measurement. (b) The experimental data and fittings of the PA measurement.

than the in-plane thermal conductivity in the "parallel" direction. This low thermal conductivity in the cross-plane direction is due to the porous and layered structure and abundant wire–wire contacts, shown in Fig. 2(b). The low thermal conductivity, combined with the high reflection surface of the silver nanowire network,[11] contribute to both thermal conduction and radiation

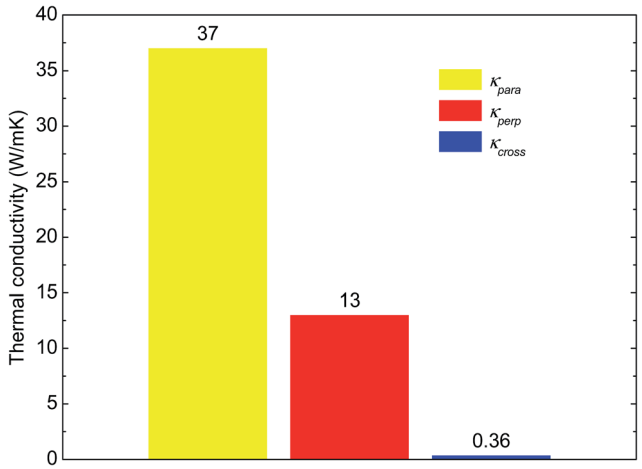

Fig. 6 The three-dimensional thermal conductivity of the nanowire film at room temperature.

insulation in the cross-plane direction. Meanwhile, high in-plane thermal conduction facilitates heat spreading, which is specifically applicable to the thermal management of flexible electronics and the functional coating of professional clothing in high- or low-temperature environments.

3.3 Quasi-ballistic electron transport and localized phonon assisted energy exchange

Electron mean free path in bulk silver at room temperature is 50 nm according to the simple kinetic theory, which is larger than the crystal sizes in silver nanowires (46 nm, 14 nm, and 11 nm in different directions according to the XRD results). As temperature decreases, the electron mean free path increases sharply in bulk silver which becomes much larger than the crystal sizes at low temperatures. When the electron mean free path is comparable or larger than the crystal sizes, electron transport in these poly-crystals are not diffusive. Electrons travel from one boundary directly to another boundary of a crystal without colliding with phonons in the crystal. During the TET measurement, most of the joule heating generates at the grain boundaries because of electron-boundary scattering when applying an electrical current. Near grain boundaries or nanowire surfaces, the generated hot electrons excite localized phonons near the boundaries. These localized phonons exchange energy mutually near the boundaries. For electron-boundary scattering, electrons are reflected back but part of their energy is transferred through the boundaries. This localized energy transfer facilitates thermal conduction while keeping charge transfer unchanged.

3.4 Lorenz number of the silver nanowire network

The temperature-dependent Lorenz numbers ($L_{\mathrm{Lorenz}} = \kappa/(T\sigma)$) of the self-assembled nanowire film in the two directions are shown in Fig. 7. The Lorenz number of bulk silver is also plotted for comparison. The Lorenz number of bulk silver is close to the Sommerfeld value ($2.44 \times 10^{-8}\ \Omega\ \mathrm{W}^{-1}\ \mathrm{K}^{-2}$) at room temperature and decreases as temperature decreases because of electron–phonon small-angle scattering. In terms of the nanowire network, we notice that both the electrical and thermal anisotropy ratios are about three and remain relatively constant as temperature decreases, indicating that size effect and wire–wire contacts dominantly impede electrical and thermal transport. Wire–wire contacts and other grain boundaries, which are structural imperfections, lower thermal and electrical conduction to the same extent. Thus, the Lorenz numbers in the two directions are the same at a certain temperature. Fig. 7 shows that at room temperature, the Lorenz number of the nanowire network is larger than the Sommerfeld value, which is due to phonon thermal conduction[35,36] and localized phonon assisted electron energy transfer. Specifically, because electrons dominate thermal conduction and the phonon contribution is small in most bulk metals, the Wiedemann–Franz law holds, and the Lorenz number is the Sommerfeld value. However, for metallic nanostructures, especially those with a large number of imperfections, the electron mean free path is limited by the structural disorder, which results in low electron thermal

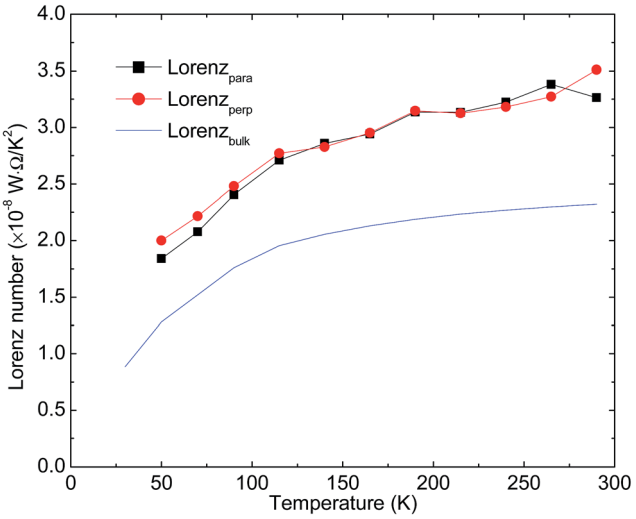

Fig. 7 The temperature-dependent Lorenz numbers of the nanowire film in the "parallel" and "perpendicular" directions. The Lorenz number of bulk silver is also plotted for comparison.[41,42]

conductivity. In this case, the phonon contribution to thermal conductivity becomes significant because of the surface phonon modes, which result in the large Lorenz number also observed in other metallic nanostructures.[35–38] Additionally, localized phonon assisted energy transfer discussed above facilitates thermal conduction while keeping electron charge transfer unchanged, which results in a large Lorenz number.

As temperature decreases from room temperature to 50 K, the Lorenz number decreases because of small-angle scattering and a reduced phonon contribution to thermal transport. At low temperatures, only phonons with small wave vectors are excited, so electron–phonon small-angle scattering dominates in electrical and thermal transport. Small-angle scattering impedes heat transport more significantly than charge transport,[37,39,40] resulting in a reduced Lorenz number. Moreover, as temperature decreases, the number of excited localized phonons decreases, which results in less electron energy transferred through boundaries by localized phonons. Additionally, the surface modes at interfaces decrease, leading to reduced specific heat and correspondingly a reduced phonon contribution to thermal conductivity. As a result, the Lorenz number of the nanowire network decreases as temperature decreases.

4. Conclusion

This paper proposed a self-assembled silver nanowire network with high thermal and electrical anisotropy with potential to solve thermal management challenges in the field of flexible electronics. In this work, the high in-plane thermal conductivity of the silver nanowire network (37 W m^{-1} K^{-1}) facilitated heat dissipation while the low cross-plane thermal conductivity (0.36 W m^{-1} K^{-1}) protected human skin or device components under the film from heating. The results suggested that size effect of silver nanowires and abundant wire–wire contacts dominantly impeded in-plane thermal transport. For thermal and electrical conduction in the in-plane directions, the excellent alignment of nanowires resulted in the same anisotropy ratio of three, which remained relatively constant as temperature decreased to 50 K, indicating that the wire–wire contacts lowered thermal and electrical conduction in both directions to the same extent and their effect was independent of temperature. In addition, phonon softening markedly reduced the Debye temperatures of the network, which were fitted from electrical resistivity data. As a result of the phonon contribution to thermal conduction and localized phonon assisted energy transfer, the Lorenz numbers of the film in the two directions, which were approximately the same, were larger than the Sommerfeld value. As the temperature decreased, the Lorenz numbers decreased because of small-angle scatterings and the reduced number of phonons. This nanowire network provides potential solutions for the thermal management of flexible electronics and the functional coatings of professional clothing.

Acknowledgements

Support of this work by National Science Foundation CMMI1264399 is gratefully acknowledged. Z. C. would like to acknowledge Prof. Zhuomin Zhang for useful discussion on localized phonon assisted energy transfer and thank Jane Chisholm for her help in technical writing.

References

1 A. L. Moore and L. Shi, *Mater. Today*, 2014, **17**, 163–174.
2 J. D. Renteria, S. Ramirez, H. Malekpour, B. Alonso, A. Centeno, A. Zurutuza, A. I. Cocemasov, D. L. Nika and A. A. Balandin, *Adv. Funct. Mater.*, 2015, **25**, 4664–4672.
3 J. A. Rogers, T. Someya and Y. Huang, *Science*, 2010, **327**, 1603–1607.
4 S. Bauer, *Nat. Mater.*, 2013, **12**, 871–872.
5 D.-H. Kim, R. Ghaffari, N. Lu and J. A. Rogers, *Annu. Rev. Biomed. Eng.*, 2012, **14**, 113–128.
6 J. J. Boland, *Nat. Mater.*, 2010, **9**, 790–792.
7 Z. Cheng, L. Liu, S. Xu, M. Lu and X. Wang, *Sci. Rep.*, 2015, **5**, 10718.
8 P. N. Nirmalraj, A. T. Bellew, A. P. Bell, J. A. Fairfield, E. K. McCarthy, C. O'Kelly, L. F. Pereira, S. Sorel, D. Morosan and J. N. Coleman, *Nano Lett.*, 2012, **12**, 5966–5971.
9 A. P. Bell, J. A. Fairfield, E. K. McCarthy, S. Mills, J. J. Boland, G. Baffou and D. McCloskey, *ACS Nano*, 2015, **9**(5), 5551–5558.
10 L. Hu, H. S. Kim, J.-Y. Lee, P. Peumans and Y. Cui, *ACS Nano*, 2010, **4**, 2955–2963.
11 P.-C. Hsu, X. Liu, C. Liu, X. Xie, H. R. Lee, A. J. Welch, T. Zhao and Y. Cui, *Nano Lett.*, 2014, **15**, 365–371.
12 D. Langley, G. Giusti, M. Lagrange, R. Collins, C. Jiménez, Y. Bréchet and D. Bellet, *Sol. Energy Mater. Sol. Cells*, 2014, **125**, 318–324.

13 H. Y. Shi, B. Hu, X. C. Yu, R. L. Zhao, X. F. Ren, S. L. Liu, J. W. Liu, M. Feng, A. W. Xu and S. H. Yu, *Adv. Funct. Mater.*, 2010, **20**, 958–964.
14 J. Guo, X. Wang and T. Wang, *J. Appl. Phys.*, 2007, **101**, 063537.
15 Z. Cheng, Z. Xu, S. Xu and X. Wang, *J. Appl. Phys.*, 2015, **117**, 024307.
16 X. Feng, X. Huang and X. Wang, *Nanotechnology*, 2012, **23**, 185701.
17 X. Feng, X. Huang and X. Wang, *Rev. Sci. Instrum.*, 2012, **83**, 044901.
18 J. Liu, Z. Xu, Z. Cheng, S. Xu and X. Wang, *ACS Appl. Mater. Interfaces*, 2015, **7**(49), 27279–27288.
19 S. Xu and X. Wang, *AIP Adv.*, 2014, **4**, 107122.
20 S. Xu, Z. Xu, J. Starrett, C. Hayashi and X. Wang, *Polymer*, 2014, **55**, 1845–1853.
21 X. Chen, Y. He, Y. Zhao and X. Wang, *Nanotechnology*, 2009, **21**, 055707.
22 X. Wang, B. A. Cola, T. L. Bougher, S. L. Hodson, T. S. Fisher and X. Xu, *Annu. Rev. Heat Transfer*, 2013, **16**, 135–157.
23 B. A. Cola, J. Xu, C. Cheng, X. Xu, T. S. Fisher and H. Hu, *J. Appl. Phys.*, 2007, **101**, 054313.
24 J. Patterson and B. Bailey, *Solid-State Physics: Introduction to the Theory*, 2nd edn, 2010, pp. 1–827.
25 A. Bid, A. Bora and A. K. Raychaudhuri, *Phys. Rev. B: Condens. Matter Mater. Phys.*, 2006, **74**(3), 035426.
26 S. Kim, H. Suhl and I. K. Schuller, *Phys. Rev. Lett.*, 1997, **78**, 322–325.
27 G. Kastle, H. G. Boyen, A. Schroder, A. Plettl and P. Ziemann, *Phys. Rev. B: Condens. Matter Mater. Phys.*, 2004, **70**(16), 165414.
28 W. Zhang, S. H. Brongersma, Z. Li, D. Li, O. Richard and K. Maex, *J. Appl. Phys.*, 2007, **101**(6), 063703.
29 G. D. Marzi, D. Iacopino, A. J. Quinn and G. Redmond, *J. Appl. Phys.*, 2004, **96**, 3458–3462.
30 W. G. Ma, X. Zhang and K. Takahashi, *J. Phys. D: Appl. Phys.*, 2010, **43**(46), 465301.
31 D.-S. Leem, A. Edwards, M. Faist, J. Nelson, D. D. C. Bradley and J. C. de Mello, *Adv. Mater.*, 2011, **23**, 4371–4375.
32 W. Gaynor, G. F. Burkhard, M. D. McGehee and P. Peumans, *Adv. Mater.*, 2011, **23**, 2905–2910.
33 E. C. Garnett, W. Cai, J. J. Cha, F. Mahmood, S. T. Connor, M. G. Christoforo, Y. Cui, M. D. McGehee and M. L. Brongersma, *Nat. Mater.*, 2012, **11**, 241–249.
34 C. Kittel, *Introduction to solid state physics*, J. Wiley, Hoboken, NJ, 8th edn, 2005.
35 N. Stojanovic, J. Berg, D. Maithripala and M. Holtz, *Appl. Phys. Lett.*, 2009, **95**, 091905.
36 S. Yoneoka, J. Lee, M. Liger, G. Yama, T. Kodama, M. Gunji, J. Provine, R. T. Howe, K. E. Goodson and T. W. Kenny, *Nano Lett.*, 2012, **12**, 683–686.
37 M. Ou, T. Yang, S. Harutyunyan, Y. Chen, C. Chen and S. Lai, *Appl. Phys. Lett.*, 2008, **92**(6), 063101.
38 H. Wang, J. Liu, X. Zhang and K. Takahashi, *Int. J. Heat Mass Transfer*, 2013, **66**, 585–591.
39 Y. Zhang, N. P. Ong, Z. A. Xu, K. Krishana, R. Gagnon and L. Taillefer, *Phys. Rev. Lett.*, 2000, **84**, 2219–2222.
40 J. M. Ziman, *Electrons and phonons: the theory of transport phenomena in solids*, Oxford University Press, 2001.
41 C. Y. Ho, R. W. Powell and P. E. Liley, *J. Phys. Chem. Ref. Data*, 1974, **3**(1), 1–796.
42 R. A. Matula, *J. Phys. Chem. Ref. Data*, 1979, **8**, 1147–1298.